Active control of 2/1 magnetic islands in a tokamak*

G. A. Navratil,[†,a)] C. Cates, M. E. Mauel, D. Maurer, D. Nadle, E. Taylor, and Q. Xiao
Department of Applied Physics, Columbia University, New York, New York 10027

W. A. Reass and G. A. Wurden
Los Alamos National Laboratory, Los Alamos, New Mexico 87545

(Received 21 November 1997; accepted 11 February 1998)

Closed and open loop control techniques were applied to growing $m/n=2/1$ rotating islands in wall-stabilized plasmas in the High Beta Tokamak-Extended Pulse (HBT-EP) [J. Fusion Energy **12**, 303 (1993)]. HBT-EP combines an adjustable, segmented conducting wall (which slows the growth or stabilizes ideal external kinks) with a number of small (6° wide toroidally) driven saddle coils located between the gaps of the conducting wall. Two-phase driven magnetic island rotation control from 5 to 15 kHz has been demonstrated powered by two 10 MW linear amplifiers. The phase instability has been observed and is well modeled by the single-helicity predictions of nonlinear Rutherford island dynamics for 2/1 tearing modes including important effects of ion inertia and finite Larmor radius, which appear as a damping term in the model equations. The closed loop response of active feedback control of the 2/1 mode at moderate gain was observed to be in good agreement with the theory. Suppression of the 2/1 island growth has been demonstrated using an asynchronous frequency modulation drive which maintains the inertial flow damping of the island by application of rotating control fields with frequencies alternating above and below the natural mode frequency. This frequency modulation control technique was also able to prevent disruptions normally observed to follow giant sawtooth crashes in the plasma core. © *1998 American Institute of Physics.* [S1070-664X(98)95705-6]

I. INTRODUCTION

Economically attractive, steady state fusion power-plant designs based on advanced tokamak physics emphasize a combination of three important features: (i) high beta, (ii) large and well-aligned noninductive bootstrap current to permit economic, steady state operation, and (iii) good confinement. The prospects for improved confinement in magnetically confined toroidal fusion plasmas has made substantial progress moving from the H (high) mode of the early 1980s to the VH (very high) mode in the early 1990s to the recent use of $E\times B$ shear to suppress turbulence in the plasma core and reduce the level of ion transport to neoclassical values in most of the plasma volume.[1] However, high beta plasmas with well-aligned bootstrap current require operation at levels of $\beta_N=10^{-8}\beta aB/I_p$ well above the beta limit for the low-n ideal kink mode.[2,3] The most promising approach to stabilize the low-n ideal kink mode is the use of a close fitting conducting wall which, if perfectly conducting, has been predicted to improve the no-wall beta limit by factors of more than 3.[2,3] Experimental studies have shown that the no-wall beta limit can be exceeded by modest factors in experiments on DIII-D[4] and on HBT-EP (High Beta Tokamak-Extended Pulse),[5] however, slower growing modes are observed to set a lower beta limit in these wall-stabilized plasmas. Since these residual modes have much slower time scales than the ideal magnetohydrodynamic (MHD) time scale for growth, they are in principle able to be actively controlled. The two most important of this class of slower growing modes are the resistive tearing mode which develops large magnetic islands resonant on magnetic surfaces inside the plasma, and the resistive wall mode[6] (RWM) which has a growth rate slowed to the resistive wall time constant and is an external mode (since its resonant surface lies in the vacuum region outside the plasma edge). This paper concentrates on experiments to control the most dangerous of these internal modes: the $m/n=2/1$ resistive tearing mode and its associated magnetic island structure. The 2/1 tearing mode has been found to play an important role in the tokamak current disruption process.

II. MODE CONTROL SYSTEMS AND BASIC PARAMETERS OF HBT-EP

The approach to mode control in HBT-EP consists of a combination of active and passive stabilization techniques. A ten-segment, adjustable conducting wall is used to provide passive stabilization of the low-n ideal kink mode. Active control of the residual slower growing 2/1 tearing mode is effected by applications of rotating helical magnetic field perturbations generated by highly modular saddle coils external to the vacuum vessel. This configuration is shown schematically in Fig. 1. The toroidal plasma has an aspect ratio, $R/a=6$ with $R=0.92$ m. The passive stabilizing conducting wall consists of ten, 1-cm-thick aluminum segments, each of which covers 26° of toroidal angle. These wall segments can be varied in radial position to study the effect of wall proximity on kink mode stabilization and these results

*gTuaI1-5 Bull. Am. Phys. Soc. **42**, 1875 (1997).
[†]Invited speaker.
[a)]Electronic mail: navratil@columbia.edu

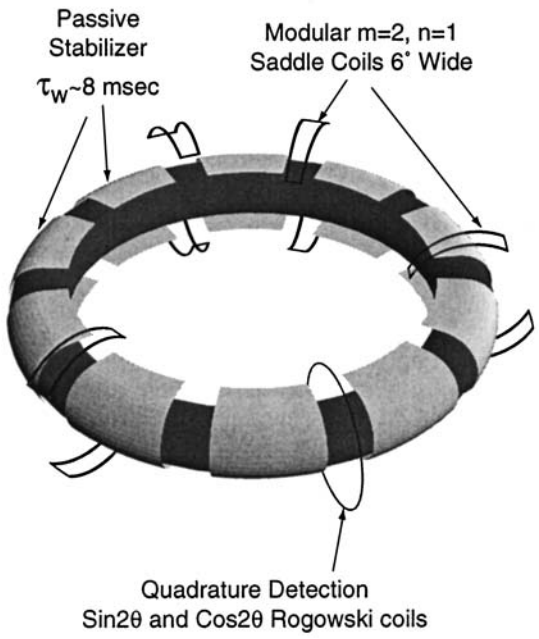

FIG. 1. Schematic of the HBT-EP control coil configuration showing ten 26° wide conducting wall segments with 6° wide $m=2$ saddle coils located at four of the 10° wide gaps in the conducting wall segments. A $\sin 2\theta$ and $\cos 2\theta$ Rogowski coil quadrature detector is located to be physically remote from the saddle coils.

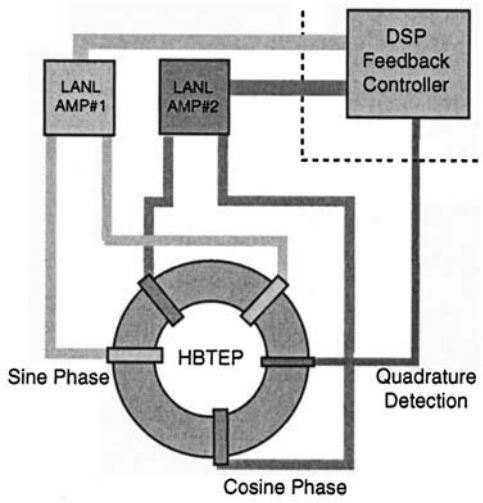

FIG. 2. Schematic of the closed loop system for mode control on HBT-EP. A digital signal processor produces phase and gain adjusted output driving two 10 MW linear amplifiers which provide a sine and cosine phase for the saddle coil generated rotating 2/1 applied field.

have been published previously.[5,7,8] In the experiments reported in this paper on active mode control of the internal 2/1 tearing modes, the wall segments were positioned less than 10% of the plasma minor radius from the plasmas edge for maximum passive stabilization of the ideal time scale modes.

A set of $m=2$ saddle coils is located at four of the 10° wide gaps in the conducting segments. Each of these saddle coils is 6° wide in toroidal angle and positioned in poloidal angle so as to couple optimally to an $m=2$, $n=1$ helical field. The saddle coils project a radial field into the plasma through 5° wide quartz toroidal gaps that allow efficient penetration of magnetic perturbations with frequencies up to 20 kHz. This highly modular configuration only covers about 3% of the toroidal surface surrounding the plasma.

Two of these saddle coils are connected in series and driven with a 10 MW linear amplifier to provide a $\sin(\omega t+\delta)$ response field and the other two coils are connected in series and driven with an independent 10 MW linear amplifier to provide a $\cos(\omega t+\delta)$ response field; together these coils provide a two-phase, quadrature winding to produce a rotating magnetic perturbation, as shown schematically in Fig. 2. The 10 MW linear amplifiers used in these experiments have a bandwidth greater than 25 kHz and can deliver ± 600 A through each of the nine-turn saddle coils. The phase and amplitude information from the rotating 2/1 island structure in the plasma is obtained from a set of $\sin 2\theta$ and $\cos 2\theta$ Rogowski coils which are physically remote (as shown in Fig. 1 and Fig. 2) from the saddle coil response fields and have very low direct pickup from the driving saddle coils. For closed loop, active mode control experiments, these $\sin 2\theta$ and $\cos 2\theta$ signal measurements are digitized by a digital signal processor (DSP) at 100 kHz and in real time ($\Delta t=10\ \mu$s) phase shifted and gain adjusted to drive the input stages of the two 10 MW linear amplifiers. These high power amplifiers provide the sine and cosine quadrature response fields that are fed back to the rotating 2/1 islands in the plasma. Shown in Fig. 3 is the relative amplitude for the $n=\pm 1$, ± 2, and ± 3 modes of the perturbed magnetic field created by a single pair of the saddle coils shown in Fig. 1, whose relative poloidal orientation is chosen to maximize the 2/1 helicity. The 2/1 helicity component is computed to be the largest, and for positive helicity modes, this is followed by the 2/2, and 2/3 modes, which we do not expect to couple strongly to the plasma.

The basic parameters of the HBT-EP tokamak are summarized in Table I. For these experiments on 2/1 mode control, the edge q value was maintained near $q\sim 2.5$ and held to values less than 3. This type of plasma produced strong naturally occurring 2/1 mode activity that began about 3 ms after

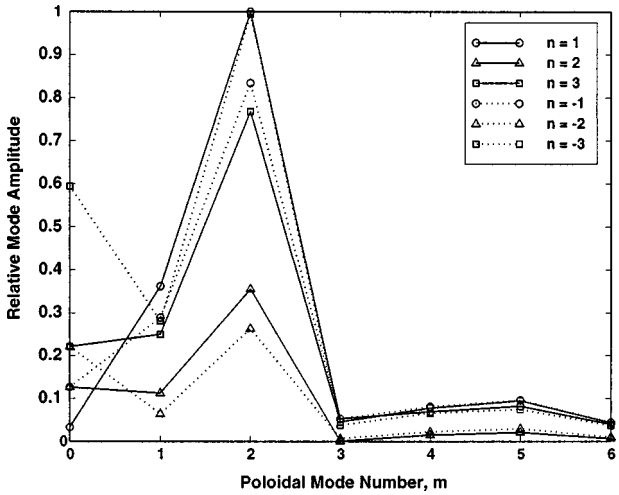

FIG. 3. Relative amplitude of the mode spectrum for $n=\pm 1$, ± 2, and ± 3 and $0\leqslant m\leqslant 6$, for a single pair of the saddle coils (sine or cosine phase) shown in Fig. 1.

TABLE I. Typical plasma parameters for HBT-EP.

Major radius, R_0	0.92–0.97 m
Minor radius, a	0.15–0.19 m
Plasma current, I_p	$\leqslant$25 kA
Toroidal field, B_T	$\leqslant$0.35 T
Pulse length	10 ms
Electron temperature, T_e	$\leqslant$80 eV average
Density, n_e	$\sim 1\times 10^{19}$ m^{-3}

plasma formation and which always led to a hard plasma disruption. The typical disruption sequence included large growth of the 2/1 islands immediately following a large sawtooth crash at about 7 ms after plasma formation resulting in prompt ($<$100 μs) loss of central temperature and significant density loss followed by a collapse of the plasma current over the following 0.5 ms. These plasmas provided a period of relatively constant amplitude saturated 2/1 activity from 3 to 7 ms and then presented a strong disruption challenge to test the robustness of any mode control scheme applied to the discharge.

III. ROTATING ISLAND MODEL EQUATIONS

To analyze our results we use the nonlinear, single-helicity model which has been built up over many years[9–14] to explain the interaction of external magnetic perturbations and a saturated tearing mode which appears as a set of rotating magnetic islands on the resonant surface in the plasma. Normalizing the mode amplitude, b, and rotation frequency, Ω, the simplified set of coupled dynamical equations for b and Ω used to model the mode control experiments described in this paper are given by

$$\frac{db}{dt} = g_1(1-\sqrt{b})\sqrt{b} + g_2\frac{b_d}{\sqrt{b}} - g_3\frac{(\Omega-1)^2}{b}, \tag{1}$$

$$\frac{d\Omega}{dt} = -h_1(\Omega-1) + h_2 b_q b - h_3\frac{\Omega\omega_0\tau_{\rm wall}}{m^2+(\Omega\omega_0\tau_{\rm wall})^2}b^2, \tag{2}$$

where, g_1, g_2, g_3, h_1, h_2, and h_3 are constants. With $W_{\rm sat}$ defined as the saturated island width, $b\equiv(W/W_{\rm sat})^2$; and $\Omega\equiv\omega/\omega_0$, where ω_0 is the natural island rotation frequency (which we measure to be primarily toroidal and in the electron drift direction). The dynamical equation for island rotation [Eq. (2)] is phenomenological as used in Ref. 9, and the size of the constants h_1, h_2, and h_3 depend upon the fraction of plasma rotating with the island. Reference 14 presents an alternate treatment of island momentum (not used here) which assumes the mass rotating with the island to be proportional to the island width.

If we further normalize time in units of ω_0, the values of the constant coefficients in Eqs. (1) and (2) are dimensionless. For example, the first terms in Eqs. (1) and (2) describe the Rutherford island growth term and a simplified, amplitude-independent relaxation of island rotation to ω_0. Defining r_s as the minor radius of the resonant tearing surface, $\tau_{\rm res}$ as the measured Rutherford growth rate, and τ_v as the measured rotational relaxation time, $g_1=2(r_s/W_{\rm sat})/\tau_{\rm res}\omega_0\sim 0.1$, and $h_1=1/\tau_v\omega_0\sim 10$.

The second terms in Eqs. (1) and (2) are the direct drive and the quadrature drive, respectively, which describe the interaction between the applied rotating helical perturbation field and the rotating 2/1 islands. The direct drive term which either increases or decreases the mode amplitude, b_d, is proportional to $I_{\rm coil}\cos(\delta)$ and the quadrature drive term is proportional to $I_{\rm coil}\sin(\delta)$ with

$$\delta \equiv \delta_0 + \int_0^t dt'(\Omega-\Omega_{\rm coil}),$$

where δ is the phase relation between the rotating island at frequency Ω and the externally applied field, $\Omega_{\rm coil}$. The dimensionless coefficients are approximately (see Refs. 9–14) $g_2\approx 2g_1/(r_s\Delta')$, and $h_2\approx(4m/\pi\alpha)(V_{\rm A}/qR\omega_0)^2\times[b_{\rm sat}/B_\theta(a)]^2\sim 10$, where $V_{\rm A}/qR$ is the characteristic Alfvén frequency, and $\alpha\leqslant 1$ represents the fraction of the plasma free to rotate with the island.

The third terms include the most important damping terms needed to fit the observed behavior of the active control experiments in HBT-EP. In Eq. (2) this damping is a wall drag term, $h_3\approx h_2(B_t/B_\theta)^2\sim 0.1$, which is small since $\omega_0\tau_{\rm wall}\sim 80$ for HBT-EP with $\omega_0\sim 6\times 10^4$ s^{-1}. In Eq. (1), this is a damping or stabilizing term on the mode amplitude found by including ion inertia and finite Larmer radius (FLR) effects, and it is quadratic in the rotation velocity difference between the island and background plasma fluid. This ion inertial stabilizing effect diminishes the mode amplitude whenever the island moves faster or slower than the background plasma toroidal rotation velocity. Defining the magnetic shear, $S=r_sq'/q$, Ref. 14 estimates the magnitude of this term for collisionless plasmas as $g_3=g_1(4/S^2)\times(R/r_s)^2(r_s/W_{\rm sat})^3(\omega_0qR/V_{\rm A})^2/(r_s\Delta')$. Depending upon the saturated island size, $r_s/W_{\rm sat}$, g_3/g_1 can range from $\sim$0.1 to approximately unity. Previous experiments on Compass-C[15] suggested that this ion inertial flow damping led to a reduction in island amplitude when a static error field was applied. We also find this term to be significant in affecting the transient island evolution in response to dynamically applied external perturbations.

IV. DRIVEN TOROIDAL ROTATION OF 2/1 ISLANDS

To benchmark the model described in Sec. III for application to the control coil geometry of HBT-EP, a series of open loop frequency ramp-up and ramp-down experiments was carried out. The results of a typical frequency ramp-up experiment are shown in Fig. 4. In this example we apply a sinusoidal current to the saddle coils and linearly advance the frequency from 2 to 15 kHz over a period of 2 ms. The phase difference between the applied magnetic field and the field of the 2/1 rotating island is shown in Fig. 4 and indicates that as the rising frequency of the applied field approaches the natural frequency of the island rotation ($\sim$8 kHz), the mode decelerates and ''locks'' to the rotating applied field at about 5 kHz. The 2/1 island is then accelerated up to about 14 kHz toroidal rotation frequency at which time the lock is lost. The

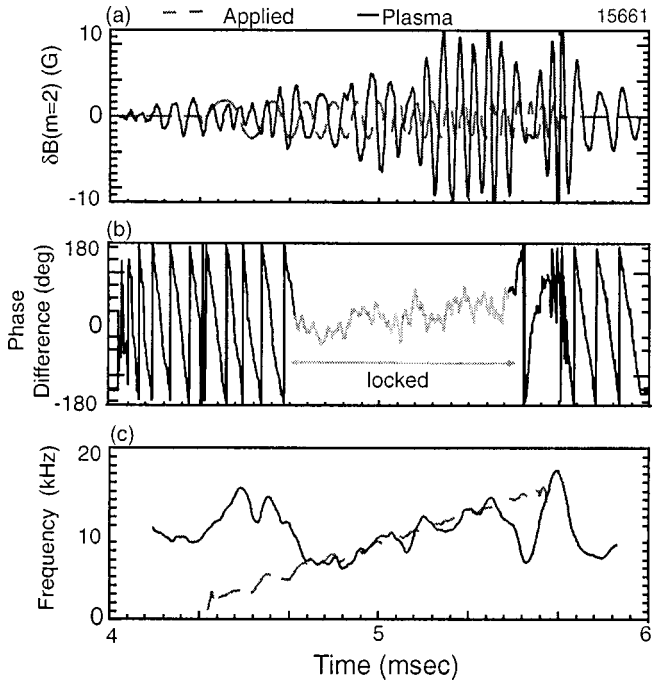

FIG. 4. Frequency ramp-up experiment from 2 to 15 kHz showing (a) the applied and plasma 2/1 mode field, (b) the phase of the 2/1 mode in the plasma relative to the phase of the applied field, and (c) the frequency of the applied field and the 2/1 mode in the plasma as a function of time.

phase difference between the driving field and mode field slowly advances from negative values to positive values as the torque demands on the driving field changes from retarding the rotation to accelerating the rotation as was reported in similar experiments on the Divertor Injection Tokamak Experiment (DITE).[10]

During the frequency ramp-up and frequency ramp-down experiments, the local ion flow velocity was measured with a Langmuir Mach probe which measures the ion fluid flow velocity near the 2/1 island. The results of this measurement are shown in Fig. 5 for both frequency ramp-up and ramp-down discharges. The ion fluid is normally observed to have a toroidal flow velocity near zero prior to mode lock, which is consistent with the picture that the ion fluid is nearly stationary due to the large charge exchange viscosity on neutrals near the plasma edge, while the mode travels with the electron fluid in the electron drift direction. In the case of the frequency ramp-up experiment of Fig. 4, the ion fluid flow velocity drops to -1 kHz when the mode frequency locks on to the applied field at 5 kHz and is accelerated to a value somewhat above zero as the mode is accelerated to near 14 kHz. The reverse is seen with the frequency ramp-down case: The ion fluid is accelerated from near zero when the mode locks on to the applied field at 14 kHz to somewhat below -1 kHz as the mode is decelerated to 5 kHz. After mode lock is lost, the ion fluid returns to near zero toroidal velocity in a few tenths of a ms. The ion fluid acceleration rate is seen here to be only about 20% of the mode acceleration rate, which is consistent with previous observations of this effect in Compass-C[15] with application of a static perturbation field and in the JAERI Fusion Torus-2M (JFT-2M)[16] with a rotating perturbation field.

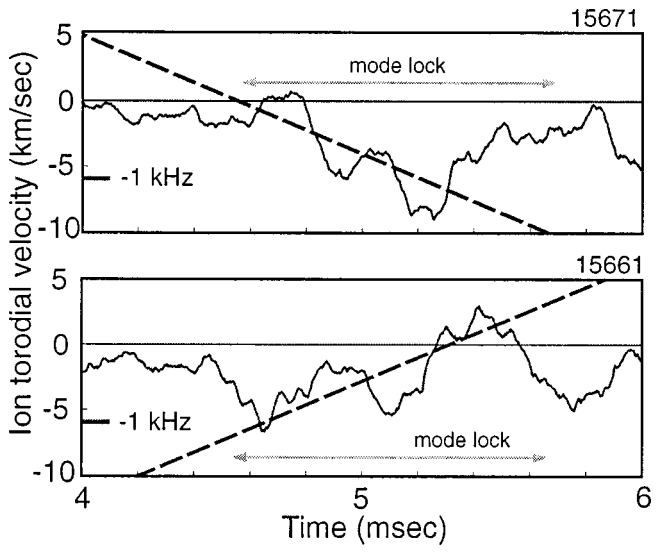

FIG. 5. Local measurement of the ion flow velocity with a Langmuir Mach probe during a frequency ramp-up and a frequency ramp-down experiment.

At the time the external field is applied in the ramp-up experiment of Fig. 4, the mode rotation frequency is briefly driven up to a large value and then relaxes back to its normal equilibrium value prior to mode lock to the applied field. We note that this kick upward in frequency is accompanied by a decrease in the mode amplitude. A similar event occurs during the loss of mode lock with a rapid drop to 7 kHz and returns to near 15 kHz which is accompanied by a drop in mode amplitude. This effect has been modeled as shown in Fig. 6 both with and without the ion inertia flow damping term in the model equations. In the case without the flow damping term included in the model, the mode is always found to lock on to the applied field and smoothly accelerate. In the case including the flow damping term, the phenomenon of a frequency excursion with associated mode amplitude reduction could be simulated, indicating that this term may play an important role in the island dynamics.

V. STUDY OF THE PHASE INSTABILITY

When the phase of an applied external field rotating with a 2/1 island is maximally stabilizing in Eq. (1), the phase of the mode relative to the applied field is in an unstable equilibrium and is subject to an unstable growth of this phase difference called the phase instability.[9] This instability can be produced in HBT-EP by applying an external 2/1 field perturbation rotating at a frequency near to the natural 2/1 island rotation frequency. The islands will immediately lock on to the applied field and grow in amplitude to a new large saturated level. If at a predetermined time the phase of the applied field is suddenly advanced by 180°, the islands will now see an applied external field which is stabilizing, resulting in a reduction in the mode amplitude and in a rapid advance in the phase of the islands in response to phase instability as the islands again move into a condition of phase lock and amplitude growth. This technique for inducing the phase instability has been employed in HBT-EP[17] and is shown in Fig. 6 together with two model simulations

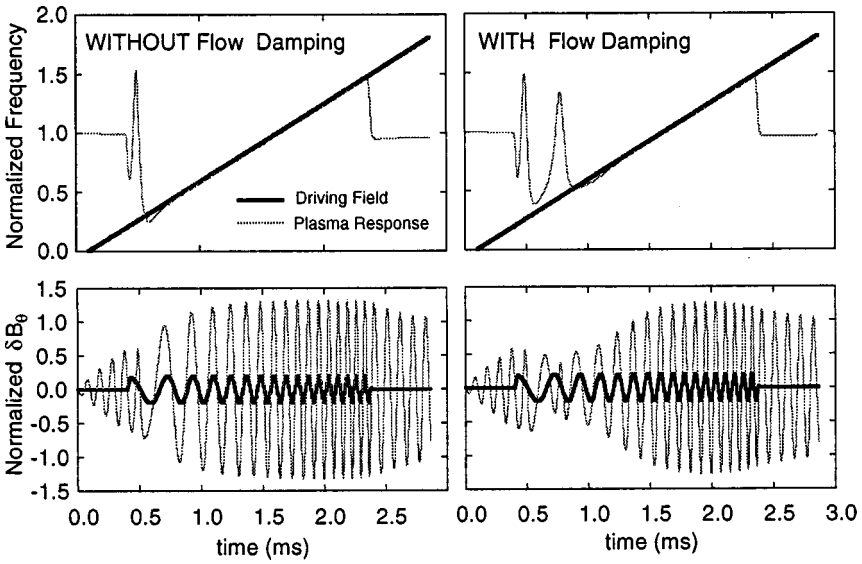

FIG. 6. Model calculation for a frequency ramp-up experiment with and without inclusion of the flow damping term in the model equations showing the time evolution of the applied 2/1 mode frequency and the applied 2/1 mode amplitude.

using Eqs. (1) and (2), one with and one without the ion inertial sheared flow damping term. Immediately after the phase change, there is a large decrease in the mode amplitude which we are unable to account for if the ion inertia stabilizing term is not included. As the island's phase advances to reestablish a phase lock with external rotting 2/1 field, a large instantaneous frequency increase occurs which causes a significant decrease in mode amplitude induced by this stabilizing effect. The coefficients used in Eqs. (1) and (2) are largely determined by experimental measurements. The coefficients g_1 and h_1 are determined by the unperturbed growth and/or decay of the island's size and rotation when the external rotating magnetic perturbation is switched off. The coefficients g_2, h_2, and h_3 are determined by the coil and wall geometry. This leaves a single parameter, g_3, to adjust until the observed decrease in island width is reproduced in the simulation. In Figs. 6 and 7, $g_3/g_1 \sim 1$, as expected for large islands.

VI. ACTIVE FEEDBACK CONTROL

By applying a rotating external 2/1 field which is maintained in a stabilizing phase relation with the mode, it is possible to use a closed loop system to carry out active feedback suppression of the 2/1 island amplitude as was demonstrated in TO-1[18] and DITE.[10] In the work reported here we carry out similar experiments, but use the highly modular saddle coil set described in Sec. II and also implement a feedback scheme similar to that proposed for use on JET (Joint European Torus)[13,19] using a fast digital signal processor. As discussed earlier in reference to Fig. 2, the quadrature detection scheme on HBT-EP measures a $\sin 2\theta$ and $\cos 2\theta$ signal giving a phase and amplitude reference for closed loop active feedback. These $\sin 2\theta$ and $\cos 2\theta$ signals are digitized at a 100 kHz rate and processed by a digital signal processor to generate a phase-shifted wave form that drives the high power amplifiers and applies a 2/1 rotating applied field with a predetermined phase shift with respect to the rotating islands. The feedback control algorithm implements a simple rotation matrix:

$$\begin{bmatrix} I_{\cos}(t+\Delta t) \\ I_{\sin}(t+\Delta t) \end{bmatrix} = G \begin{bmatrix} \cos(\delta) & -\sin(\delta) \\ \sin(\delta) & \cos(\delta) \end{bmatrix} \begin{bmatrix} B_{\cos 2\theta}(t) \\ B_{\sin 2\theta}(t) \end{bmatrix}. \quad (3)$$

This scheme is designed to maintain a constant phase relation between the detected mode phase and applied external rotating field.

We can model the expected equilibrium response of the 2/1 islands by setting the time derivatives to zero in Eqs. (1) and (2). Assuming that $\Omega\ \omega_0\tau_{\text{wall}} \gg 1$ we solve the following coupled nonlinear equations for the expected mode amplitude and frequency as a function of phase angle and closed loop system gain, G:

$$0 = g_1(1-\sqrt{b})\sqrt{b} + g_2 G\ \cos(\delta)\sqrt{b} - g_3\frac{(\Omega-1)^2}{b}, \quad (4)$$

$$0 = -h_1(\Omega-1) + h_2 G\ \sin(\delta) b - \frac{h_3 b^2}{\Omega\omega_0\tau_{\text{wall}}}. \quad (5)$$

Assuming moderate system gain the variation expected in Ω and b are plotted in polar form for variations in δ in Fig. 8. The mode is reduced in amplitude for $\delta = 0°$ and driven to larger amplitude for $\delta = 180°$. For phase angles of 90° and 270° the amplitude is little changed, but we expect a higher frequency at $\delta = 90°$ and a lower frequency when $\delta = 270°$. If the normalized mode frequency is reduced to values of about 0.5 by the active control loop, the mode is predicted to lock to $f = 0$ in the lab frame. This mode locking is most likely at about 230° and has been observed in the experiments on HBT-EP when the gain is increased. The effect is due to a nonlinear interaction between the mode amplitude which is directly proportional to the torque applied by the driving field and the ion inertial damping which scales quadratically with the frequency and inversely with the mode amplitude.

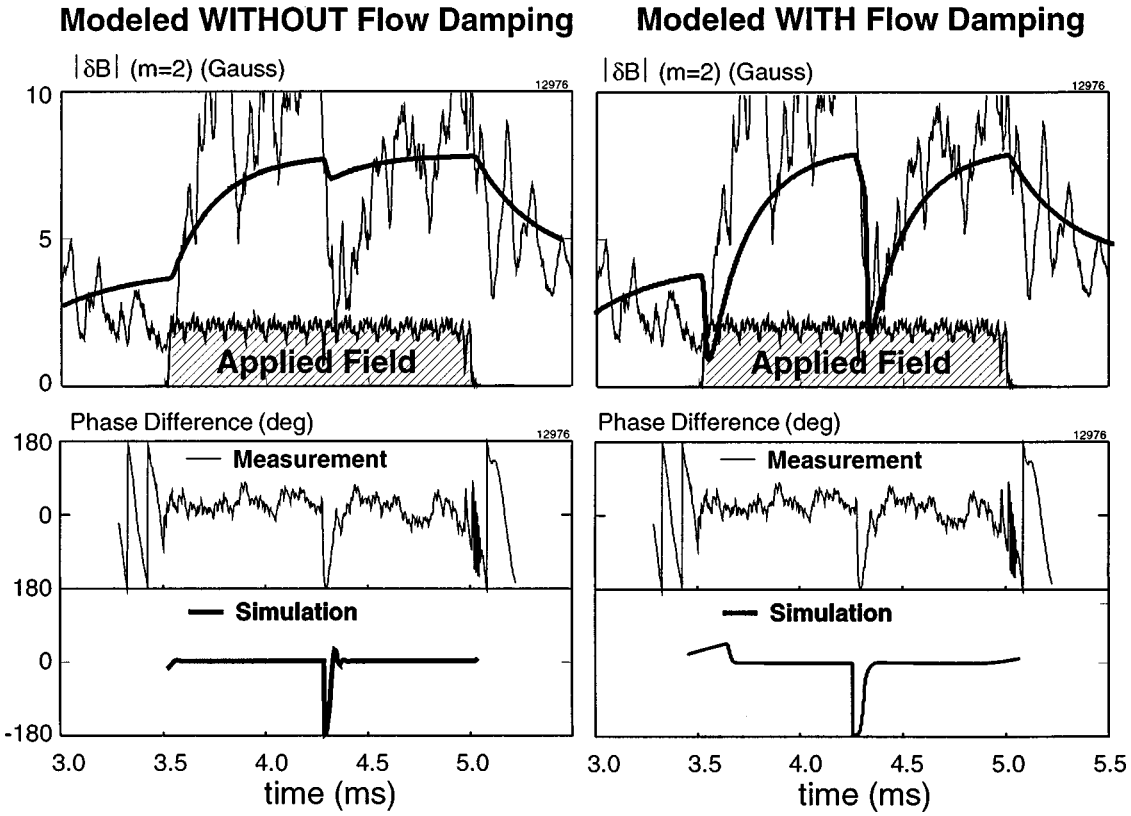

FIG. 7. Measurement of the phase instability when the toroidal phase of a rotating magnetic perturbation is suddenly advanced by 180°. The time history of the measured amplitude and phase of the 2/1 island is shown compared with simulation calculations with and without the flow damping term in the model equations.

Closed loop experiments were carried out for $\delta=0°$ and 180° on a single discharge with the stabilizing phase angle applied for 1 ms followed by the destabilizing phase angle applied for the following 1 ms. These results are shown in Fig. 9 showing the time history of the applied phase angle, δ, the amplitude of the sine and cosine phase of the 2/1 islands, and the frequency of the island rotation. During the 1 ms application of the stabilizing phase angle, the frequency is observed to rise from about 7 to 10 kHz with a relatively constant amplitude. After the transition to the destabilizing phase angle, the mode amplitude is observed to grow larger and the frequency of the mode is observed to decline from 10 to 7 kHz in agreement with the expectations of the equilibrium model of Eqs. (4) and (5). If the data are averaged over 0.1 ms intervals and plotted against the predictions of the model, we find reasonably good agreement as also shown in Fig. 9.

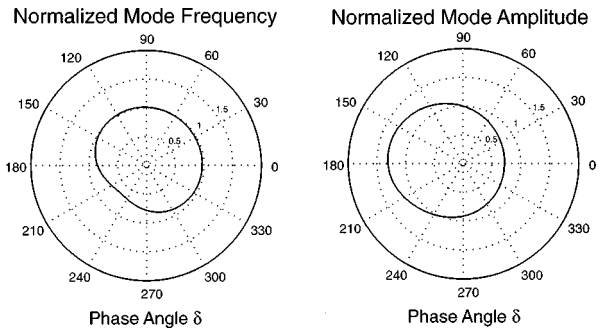

FIG. 8. Results of the equilibrium model calculations Eqs. (4) and (5) as a function of phase angle for moderate gain.

A similar experiment can be carried out for the phase angles $\delta=270°$ and 90° where we expect a frequency decrease and frequency increase. The results of this experiment are shown in Fig. 10. During the initial application of the frequency decrease phase angle, we see the frequency maintained at about 7 kHz. After the transition to the frequency increase phase angle, the island rotation frequency is observed to increase to about 9 kHz over a period of 1 ms. These results are also plotted averaged over 0.1 ms intervals against the model predictions showing good agreement.

When the gain of the feedback system is increased to achieve a larger suppression of the mode amplitude or to attempt to control the 2/1 island size immediately prior to the normal strong growth phase prior to disruption, we find that phase accuracy of the response field is degraded and the closed loop system is no longer able to maintain a specified stabilizing phase angle. This effect appears to be due to the large phase angle delay inherent in the system using a 100 kHz digitization rate and a 10 μs delay in computing the next wave form update. The zero-order hold digital delay used on the output combined with the 100 kHz data acquisition rate, results in a frequency-dependent phase delay of more than 50°. Given the higher growth rate for the phase instability as the system gain is increased as well as the large frequency changes which can occur as the mode amplitude grows prior to disruption, the 100 kHz digital signal processing system was unable to maintain phase lock on the mode. As expected

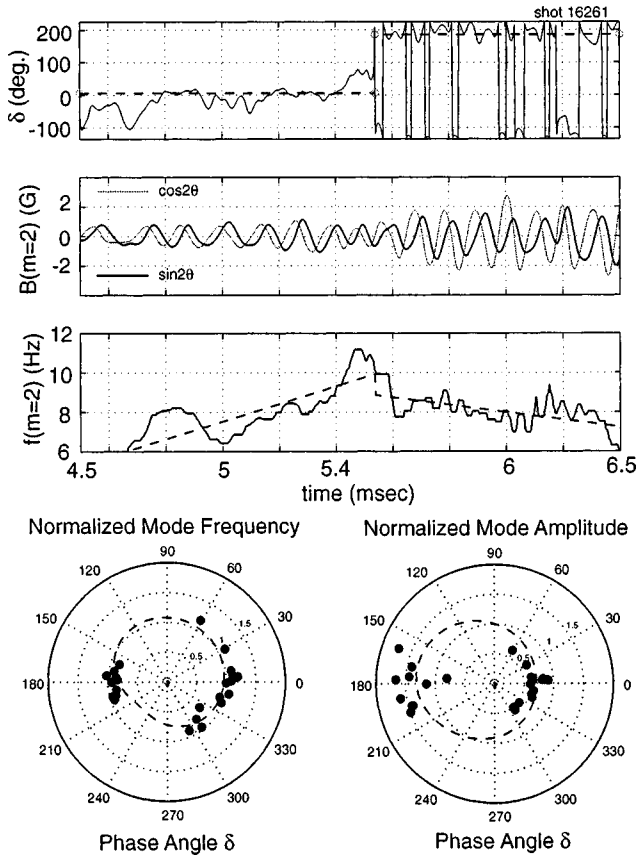

FIG. 9. Application of stabilizing (0°) phase and destabilizing (180°) phase each for 1 ms compared with the results of the equilibrium model shown in Fig. 8.

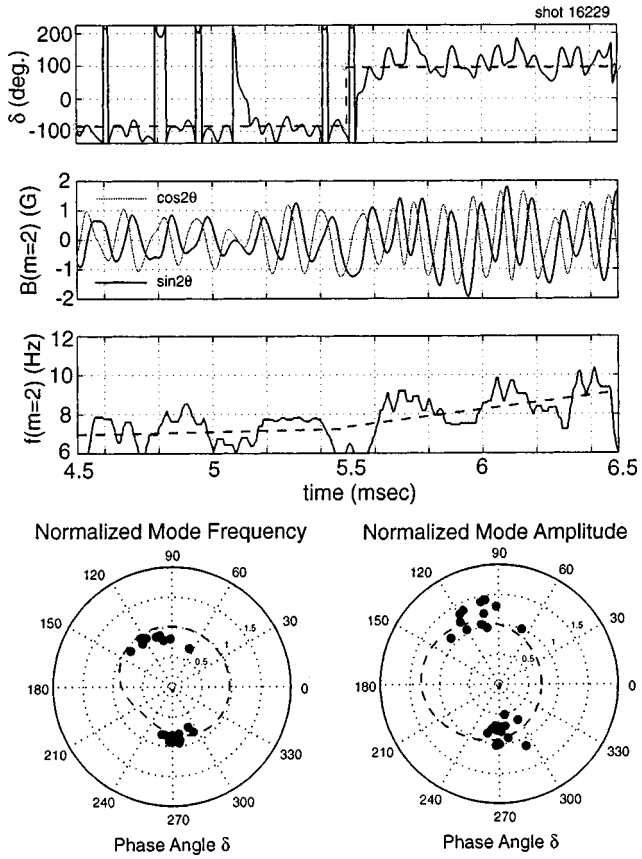

FIG. 10. Application of frequency downshift (270°) phase and frequency upshift (90°) phase each for 1 ms compared with the results of the equilibrium model shown in Fig. 8.

in light of the difficulties in maintaining a phase reference for the applied external rotating 2/1 field, tests of the system at high gain during the period of large 2/1 island growth immediately prior to disruption showed no effect on the disruption timing or severity.

VII. FREQUENCY MODULATION STABILIZATION

Since we have observed in the frequency ramp and phase instability model benchmark experiments described in Secs. IV and V, a significant role played transiently by ion inertia flow stabilization in reducing the island amplitude, experiments were carried out to induce this effect over an extended period. The use of time averaged flow stabilization to control the average mode amplitude was originally proposed by Kurita *et al.*,[20] who simulated the effect of modulation of an applied external rotating resonant field whose frequency was modulated alternately above and below the normal mode rotation frequency. Since the response of the rotating island to such an external field is to increase or decrease the rotation frequency in order to establish a phase lock on the applied field, this should result in a reduction in the mode amplitude during the periods where the $(\Omega-1)^2$ ion inertia flow damping term in Eq. (1) becomes larger. By choosing the duration of the alternating high and low frequency periods to be sufficiently short so that mode lock is avoided, a time average reduction in the 2/1 island amplitude should be obtained. Shown in Fig. 11 are the results of a simulation of this effect using parameters in the model Eqs. (1) and (2) which were benchmarked against the previous frequency ramp, phase instability, and active feedback experiments. Assuming a normal island rotation frequency of 10 kHz, a 2/1 rotating field was applied with a frequency of 15 kHz alternating with 5 kHz every 0.2 ms. We can see from the results of the simulation, that if the ion inertia flow stabilization term is not included in the model, the mode rapidly locks on to the applied field and grows to relatively large amplitude. On the other hand, when this stabilizing term is included, the islands do not achieve phase lock and the mode amplitude is observed to saturate at a much lower average amplitude.

The frequency modulation stabilization experiment modeled above was carried out in HBT-EP and the results are summarized in Fig. 12. Shown in the figure is the application of the alternating 5 and 15 kHz externally applied 2/1 drive field together with the response of the island rotation frequency. As the frequency of the applied field alternates, the rotating island toroidal velocity is strongly modulated and a phase lock with the applied field is avoided. Also plotted in Fig. 12 is the $(\Omega-1)^2$ ion inertia flow damping term based on the actual mode rotation frequency. During times when the values computed for $(\Omega-1)^2$ are relatively large compared with the measured 2/1 island amplitude they are found to correlate with a reduction in mode amplitude.

Most significantly, when this frequency modulation stabilization technique is applied at the end of the discharge

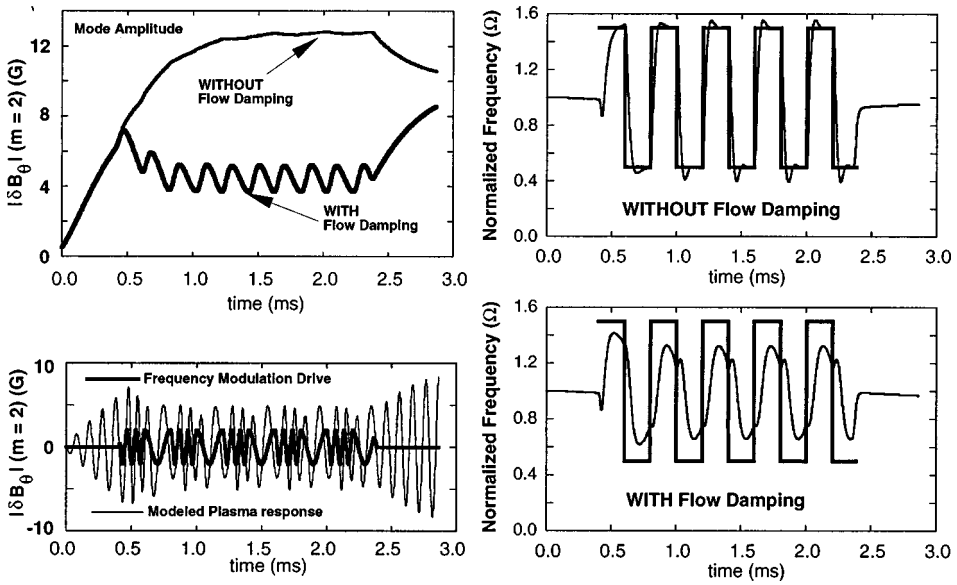

FIG. 11. Simulation of the effect on the mode amplitude and mode frequency in response to frequency modulation of the applied field with 5 and 15 kHz applied for 0.2 ms alternately. The simulation illustrates the result of including the effect of flow damping in the model equations.

when the development of very large sawteeth normally leads to a hard disruption, the hard disruption was prevented and the discharge lifetime was extended. These results are shown in Fig. 13 for two discharges with edge $q\sim 2.5$, one with the frequency modulation stabilization applied and a very similar reference shot without frequency modulation stabilization. In the case of the reference shot 16 389, we see that central soft x-ray emissivity rises in time until a very large sawtooth collapse occurs at about 6.6 ms with an associated loss of half the line integrated plasma density, and disruption of the plasma current which begins to collapse immediately. When the frequency modulation stabilization was applied in shot 16 411 for a 3 ms period beginning at 4.5 ms, we see that this discharge also suffers a large sawtooth collapse at about the same time as the reference shot 16 389, however, in this case the plasma density and plasma current continue showing little or no effect. This appears to be due to preserving the integrity of the outer flux surfaces by frequency modulation control of the 2/1 island size. The plasma core temperature begins to recover after the sawtooth collapse and a second large sawtooth even occurs, again without loss of outer flux surface confinement or disruption of the plasma current.

The frequency modulation stabilization is turned off at 7.5 ms, and almost immediately ($\lesssim$0.1 ms) the plasma suffers a hard disruption of the current and loss of plasma density. In contrast to the usual disruption sequence for these plasmas which initiate with a large central collapse of the soft x-ray emissivity, followed by growth of the 2/1 islands and then current disruption, in this frequency modulation sta-

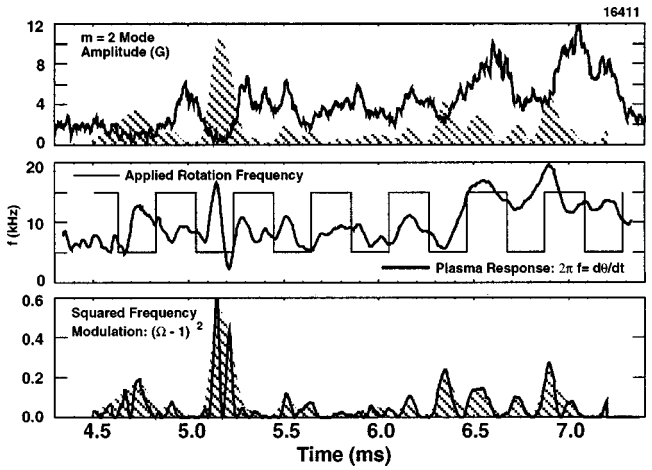

FIG. 12. Results of experiment using frequency modulation of the applied field with 5 and 15 kHz applied for 0.2 ms alternately. The squared frequency modulation $(\Omega-1)^2$ (referenced against a 0.4 ms boxcar averaged frequency) is compared with the mode amplitude.

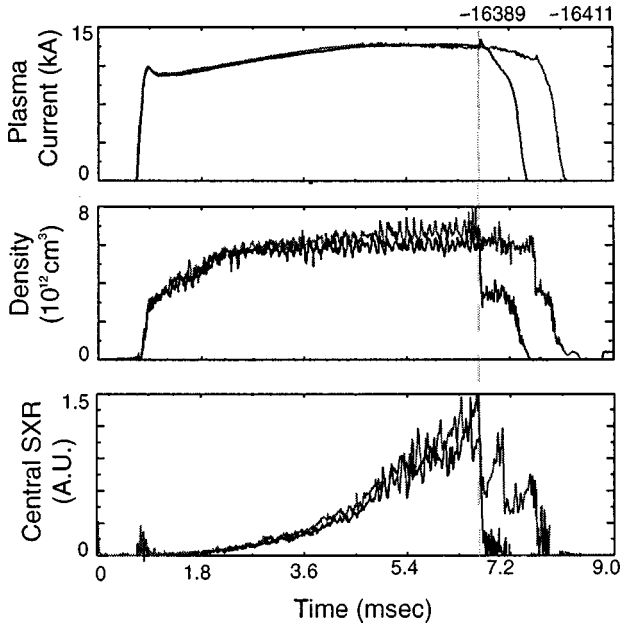

FIG. 13. Disruption control demonstration of frequency modulation (FM) suppression. A disruptive reference shot 16 389 is compared with a similar shot 16 411 with FM suppression applied which does not disrupt in response to several large sawteeth events.

bilized plasma the current and density loss disruption actually precedes the central soft x-ray collapse, indicating the disruption event was initiated by loss of outer flux surface confinement shortly after the frequency modulation was switched off. It has also been observed that application of a predominantly $2/-1$ nonresonant helicity with the same amplitude and modulated frequency shows no coupling to the 2/1 mode and no measurable effect on the plasma.

VIII. SUMMARY AND DISCUSSION

Closed and open loop control techniques were applied to growing $m=2$, $n=1$ rotating islands in wall-stabilized plasmas in the HBT-EP tokamak. The approach taken by HBT-EP combines an adjustable segmented conducting wall (which slows the growth or stabilizes ideal external kinks) with four highly modular (6° wide toroidally) saddle coils located between the gaps of the conducting wall and covering only about 3% of the plasma surface. The success of these experiments provides a basis for consideration of systems with greater modularity and localization. The installation of extensive internal coils sets in larger tokamaks is technically difficult and the higher frequency response coils needed for control of internal modes prevents their location behind passive stabilization structures needed to deal with low-n ideal kink modes. The option of a highly modular configuration in conjunction with a segmented passive stabilizer may allow the possibility of active control of internal and external modes on medium scale experiments such as DIII-D and the National Spherical Tokamak Experiment (NSTX)[21] as well as even in larger scale devices like the International Thermonuclear Experimental Reactor (ITER).[22]

In this paper we described experiments which demonstrate two-phase island rotation control from 5 to 15 kHz and the observation of the phase instability, both of which are well modeled by the single-helicity predictions of nonlinear Rutherford island dynamics for 2/1 tearing modes. These model equations include important effects of ion inertia and FLR which appear as a quadratic flow damping term scaling like $(\Omega-1)^2$ for the mode amplitude. We find this to be an important term in modeling the observations of driven rotation and the phase instability. Induced ion flow was observed with local Langmuir Mach probes during the two-phase island rotation drive experiments with the rate of ion fluid acceleration equal to about 20% of the rate of the island acceleration. The normal ion fluid flow velocity is nearly zero and rotation rates somewhat larger than -1 kHz were measured relative to the island rotation direction.

The closed loop response of active feedback control of the 2/1 mode at moderate gain was observed to be in good agreement with the theory when the phase angle of the applied field was varied relative to the 2/1 island. However, at high system gain stable phase control was not achieved and a higher digitization rate and faster digital signal processing system will be necessary. As a consequence the effects on the disruption process through control of the 2/1 island amplitude have not yet been demonstrated for this mode control technique.

Experiments have been carried out which show suppression of the 2/1 island growth using an asynchronous frequency modulation drive which maintains the ion inertial effect of flow damping. Originally suggested and modeled by Kurita *et al.*,[20] we apply asynchronous external 2/1 control fields at frequencies alternatively above and below the natural mode frequency. Previous experiments have not had the capability to modulate the frequency of the rotating mode sufficiently fast to observe significant damping from this flow stabilizing effect. The frequency modulation control technique was also able to prevent disruptions normally observed to follow giant sawtooth crashes in the plasma core. By preventing the uncontrolled growth of the 2/1 island following a large sawtooth as normally occurs, the confinement of the outer flux surfaces was preserved and the disruption was prevented, allowing the plasma core to re-heat.

ACKNOWLEDGMENTS

This research is supported by Department of Energy Grant No. DE-FG02-86ER53222. The authors also gratefully acknowledge the technical support provided by M. Cea, N. Rivera, and E. Rodas.

[1] E. A. Lazarus, G. A. Navratil, C. M. Greenfield *et al.*, Phys. Rev. Lett. **77**, 2714 (1996).
[2] C. Kessel, J. Manickam, G. Rewoldt, and W. Tang, Phys. Rev. Lett. **72**, 1212 (1994); J. Manickam, M. S. Chance, S. C. Jardin *et al.*, Phys. Plasmas **1**, 1601 (1994).
[3] A. Turnbull, T. S. Taylor, Y. R. Lin-Liu, and H. St. John, Phys. Rev. Lett. **74**, 718 (1995).
[4] T. Taylor, E. J. Strait, L. L. Lao *et al.*, Phys. Plasmas **2**, 2390 (1995).
[5] T. Ivers, E. Eisner, A. Garafalo *et al.*, Phys. Plasmas **3**, 1926 (1996).
[6] J. P. Freidberg, *Ideal Magnetohydrodynamics* (Plenum, New York, 1987).
[7] D. A. Gates, Ph.D. thesis, Columbia University, 1993, Columbia Plasma Physics Laboratory Report No. 127.
[8] A. Garofalo, Ph.D. thesis, Columbia University, 1997, Columbia Plasma Physics Laboratory Report No. 130.
[9] E. Lazzaro and M. F. F. Nave, Phys. Fluids **31**, 1623 (1988).
[10] A. W. Morris, T. C. Hender, J. Hugill *et al.*, Phys. Rev. Lett. **64**, 1254 (1990).
[11] R. Fitzpatrick and T. C. Hender, Phys. Fluids **3**, 644 (1990).
[12] G. Bosia and E. Lazzaro, Nucl. Fusion **31**, 1003 (1991).
[13] G. D'Antonia, IEEE Trans. Nucl. Sci. **41**, 216 (1994).
[14] A. I. Smolyakov, A. Hirose, E. Lazzaro, G. B. Re, and J. D. Callen, Phys. Plasmas **2**, 1581 (1995).
[15] T. C. Hender, R. Fitzpatrick, A. W. Morris *et al.*, Nucl. Fusion **32**, 2091 (1992).
[16] K. Oasa, H. Aikawa, Y. Asahi *et al.*, *Plasma Physics and Controlled Nuclear Fusion Research 1994*, Proceedings of the 15th International Conference, Seville (International Atomic Energy Agency, Vienna, 1995), Vol. 2, p. 279.
[17] M. E. Mauel, E. Eisner, A. Garofalo *et al.*, *Plasma Physics and Controlled Nuclear Fusion Research 1996*, Proceedings of the 16th International Conference, Würtzburg (International Atomic Energy Agency, Vienna, 1997), Vol. 1, p. 731
[18] V. V. Arsenin, L. I. Artemenkov, N. V. Ivanov *et al.*, *Plasma Physics and Controlled Nuclear Fusion Research 1978*, Proceedings of the Seventh International Conference, Innsbruck (International Atomic Energy Agency, Vienna, 1979), Vol. 1, p. 233.
[19] R. Savrukhin, D. J. Campbell, G. D'Antona, and A. Santagiustina, IEEE Trans. Plasma Sci. **43**, 238 (1996).
[20] G. Kurita, T. Tuda, M. Azumi, and T. Takeda, Nucl. Fusion **32**, 1899 (1992).
[21] M. Ono and The NSTX Team, Bull. Am. Phys. Soc. **42**, 1988 (1997).
[22] ITER-JCT and Home Teams, Plasma Phys. Controlled Fusion **37**, A19 (1995).